



Na₃Fe₂(SO₄)₂(SO₃N) as a potential high capacity cathode material



Bruno Rousseau^{a,b}, Vladimir Timoshevskii^a, Normand Mousseau^b, Michel Côté^b, Karim Zaghib^{a,*}

^a Direction de Stockage et Conversion de l'Énergie (SCE), Institut de Recherche d'Hydro-Québec (IREQ), 1800 boul. Lionel-Boulet, Varennes, QC J3X 1S1, Canada

^b Regroupement Québécois sur les Matériaux de Pointe (RQMP), et Département de Physique, Université de Montréal, C. P. 6128, Succursale Centre-Ville, Montréal, Québec H2C 3J7, Canada

ARTICLE INFO

Article history:

Received 15 April 2016

Received in revised form 21 June 2016

Accepted 12 July 2016

Available online 18 July 2016

Keywords:

Sodium battery

Sulfate cathode

Nitrogen doping

Density functional theory

ABSTRACT

A novel sulfate material, Na₂Fe₂(SO₄)₃, was recently proposed as a high-density cathode material for sodium-based batteries (Barpanda et al., 2014). This study presents *ab initio* simulations describing the effect of partial oxygen-to-nitrogen substitution in this material with the aim of increasing the sodium capacity of the structure as well as its energy density. The considered structure with the most likely substitution configuration increases the theoretical energy density to 650 W h kg⁻¹, improving over the theoretical value of 480 W h kg⁻¹ for the original, nitrogen-free structure.

© 2016 Elsevier B.V. All rights reserved.

1. Introduction

Electrochemical energy storage is an essential component of many modern technologies, from portable electronic devices to electric cars. The pioneering experimental studies of the complex oxide compounds [2,3] suggest that these systems could meet the energy storage demand for these usages effectively and safely. As materials improvements lead to reduced costs, massive grid-scale electrochemical storage also becomes an economically viable pathway to decouple electrical energy production and consumption, allowing the large-scale use of intermittent renewable energy. These two broad classes of storage applications, mobile and immobile, have different critical requirements: mobile storage must maximize energy density by weight whereas large-scale immobile storage demands low costs and long material lifetimes. While the need for cheap and energy dense materials remains strong, it is feared that lithium-ion-based technologies, currently dominating portable device markets, are now mature and can only offer at most 30% improvement in energy density by weight [4]: the next generation of energy storage materials may well lie beyond the Li ion-transition metal redox paradigm.

One route departing from this paradigm and receiving renewed attention is that of sodium ions in intercalation compounds [5–7]. It is sometimes believed that sodium leads to lower voltages because its anodic half-cell potential is 0.33 V higher than that of lithium. Yet, this reasoning is misleading [8] and the recent synthe-

sis and characterization of a novel sulfate, Na₂Fe₂(SO₄)₃, utilizing the Fe²⁺/Fe³⁺ redox level and exhibiting an average intercalation voltage of 3.8 V, is a remarkable counter-example to this affirmation [1]. The reported structure of Na₂Fe₂(SO₄)₃ (NFS) offers three distinct Na sites per formula unit where only two of these are occupied on average, leading to a moderate experimental charge capacity of ~100 mA h g⁻¹.

Another route to improvement, which has emerged recently, is the partial oxidation of anions in intercalation compounds to increase capacity. Indeed, the reversible oxidation of oxygen (i.e., O²⁻ → ½ O₂²⁻ + e⁻) has been proposed as the underlying mechanism explaining the higher-than-expected capacities of certain layered oxides [9] upon lithium de-intercalation. It has also been suggested that partially substituting oxygen with nitrogen in Li₂FeSiO₄ may allow the extraction of more than one Li per formula unit [10,11].

In this work, we seek to combine the two routes presented above by considering oxygen-to-nitrogen substitution in NFS in order to increase capacity without jeopardizing the high voltage of the original structure.

2. Methodology

Simulations of a number of NFS variants with nitrogen substituents were conducted using the Vienna *Ab initio* Simulation Package (VASP) [12] at the level of GGA+U exchange-correlation functional [13–16], which partially corrects for the shortcomings of GGA for the correlation energy of *d*-electrons. Values of *U* as parametrized by Wang et al. were used [17,18] along with the

* Corresponding author.

E-mail address: Zaghib.Karim@ireq.ca (K. Zaghib).

PAW formalism with high-quality pseudopotentials [19,20]. All computations were performed with an energy cutoff of 520 eV and a $4 \times 4 \times 4$ Monkhorst-Pack k -grid. The structures were relaxed until the largest residual force was smaller than 5×10^{-2} eV \AA^{-1} . The thermodynamic stability of the various proposed modifications was assessed by comparing their total energies to the total energies of all possible decomposition products available through the Materials Project online database [18]. Voltages were computed by comparing the most stable total energies of partially sodiated structures [8,21]. Simulations and data analysis were conducted with the help of software related to the Materials Project [22,23].

3. Results and discussion

NFS has either space group symmetry $P2_1/C$ or $C2/c$, the former fitting experimental observations only slightly better than the latter [1]. The two structures are very similar but the $C2/c$ structure is computationally more convenient, as it counts two formula units per unit cell instead of four for the $P2_1/C$ structure, reducing computational efforts; it will thus be used as a starting point, a choice that should not affect the overall results since the two structures are close. As can be seen in Fig. 1, the $C2/c$ structure is composed of pairs of edge-sharing FeO_6 octahedra arranged in layers and joined by intra- and interlayer SO_4 tetrahedra. These layers, as schematically represented in Fig. 1(a), are stacked in an AB arrangement shown in Fig. 1(b). The interlayer sulfate groups joining the octahedral from different layers leave large channels where the sodium ions can readily intercalate. In the original structure reported by Barpanda et al. [1], there are three symmetrically distinct sites for Na per formula unit, two of which are occupied on average in the fully sodiated structure. The oxygen, for its part, occupies a variety of chemical environments within the structure. As can be seen in Fig. 1(b), the oxygen cation can belong to an interlayer tetrahedron or to an intralayer tetrahedron, connecting to either zero [dangling], one [intralayer(1)] or two [intralayer(2)] Fe ions. As will be discussed later, the sites labeled “ N_2 bond” are two intralayer(1) sites which are close enough to form N-N bond upon desodiation if both sites are substituted with nitrogen.

Nitrogen is introduced by the substitution of one SO_3N per formula unit, resulting in $\text{Na}_3\text{Fe}_2(\text{SO}_4)_2(\text{SO}_3\text{N})$, a substitution that could be made possible experimentally thanks to a recent method introducing this polyanion in compounds [24]. A high specific capacity could thus be achieved by complementing the $\text{Fe}^{2+}/\text{Fe}^{3+}$

redox with the oxidation of the N^{3-} anion [11]. There are two formula units per unit cell in the $C2/c$ structure, implying 6 distinct SO_4 tetrahedra. Picking 2 tetrahedra out of 6 and accounting for 4 possible sites per tetrahedron leads to 240 possible fully sodiated structures; a careful accounting of all point symmetries reduces this number to 68 truly distinct substituted structures.

The total energy of all 68 structures was computed and is presented in Fig. 2(a), showing that interlayer positions for N are most stable, followed by intralayer(2) and intralayer(1), and that substituting a dangling oxygen for a nitrogen is least stable. Three structures labeled A, B and C were selected for further analysis; the corresponding substitution patterns can be seen in Fig. 2(b), (c) and d (d), respectively. The structures A and B were chosen for being the most stable structures with interlayer and intralayer substitutions; structure C is also considered because it is the only structure that allows the formation of N_2 pairs upon desodiation, as can be seen in Fig. 2(d). Indeed, all intralayer(1)-intralayer(1) structures of energy lower than C either have their nitrogen substitutes too far from each other to realistically form a bond, or undergo a relaxation of the fully desodiated structure where the N-N distance remains large.

The computed voltage profiles for structures A, B and C are compared to that of NFS in Fig. 3(a). These average computed voltages are obtained by considering the energy of every possible intermediate level of sodiation for a given structure while maintaining the original translational symmetry, keeping only the most stable energies for partially sodiated structures. All these energies, expressed relatively to that of a mixture of the corresponding fully sodiated and fully desodiated structures, are presented in Fig. 3 (c), (d), (e) for structures A, B and C respectively. The thermodynamic stability energy of every partially sodiated structure belonging to a convex hull is presented in Fig. 3(b) where a negative value indicates thermodynamic stability and a positive value corresponds to the structure's excess energy when compared to a mixture of correct stoichiometry of all known compounds.

Structures A and B have qualitatively similar properties. Computed voltages decrease monotonously from ~ 4.5 V when structures are desodiated to about 2.7 V in the fully sodiated structures, a result comparable to the computed voltage profile of NFS. Whereas fully sodiated NFS is found to be thermodynamically stable, the introduction of nitrogen leads to excess energies of about 60 meV per atom. This does not preclude dynamical stability, however, as no information is available on the energetic barriers to structural changes that could occur.

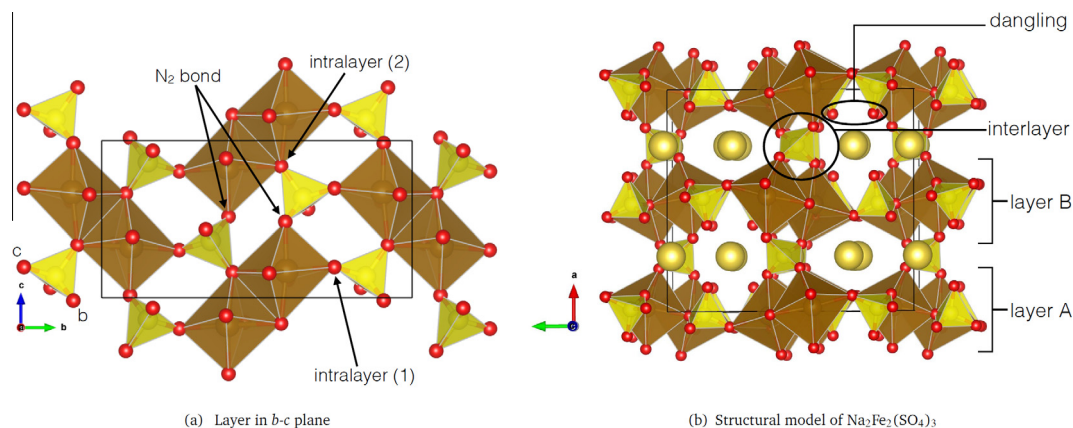


Fig. 1. Visualization of the structure proposed by Barpanda et al. [1] with $C2/c$ symmetry in an almost orthorhombic supercell shown for clarity. (a) View of the layers lying in the b - c plane, with various oxygen sites identified; (b) view normal to the a - b plane. Small red spheres represent oxygen, yellow tetrahedra represent sulfate groups and iron atoms are at the center of brown octahedra. The yellow spheres represent sodium ions. (For interpretation of the references to color in this figure legend, the reader is referred to the web version of this article.)

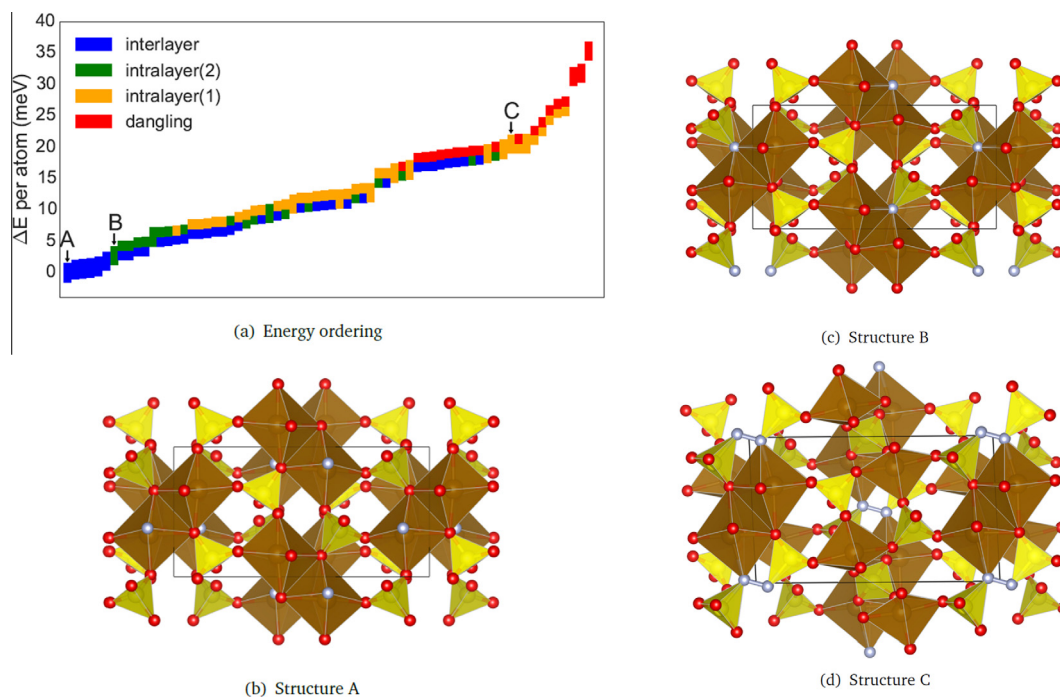


Fig. 2. (a) Computed total DFT+U energy per atom for all nitrogen substituted structures of the form $\text{Na}_3\text{Fe}_2(\text{SO}_4)_2(\text{SO}_3\text{N})$, relative to the most stable structure (labeled A). The primitive unit cell contains two formula units, and thus there are two N per cell; the color code represents the family of each substituted site. Structures for which voltage curves were computed are identified by A, B and C. (b), (c), (d) Structural model for relaxed desodiated structures corresponding to A, B and C. Small grey spheres represent nitrogen. (For interpretation of the references to color in this figure legend, the reader is referred to the web version of this article.)

Finally, the magnetizations of every Fe ion in the unit cells of structures on convex hulls are presented in Fig. 3(f), (g) and (h). These magnetizations can be used as an approximate proxy for the redox state of the Fe ions. As an electron arrives from the external network to the cathode site during the discharge process, it can localize on one of Fe atoms, changing its ionic state from 3+ to 2+. The corresponding change of the electronic configuration of Fe ion is from $3d^5$ to $3d^6$. Due to the localized nature of Fe d -electrons in this compound, each of these configurations features a particular spin magnetic moment, which is higher for 3+ state and lower for 2+ state. This makes local magnetic moment (in case of localized d -electrons) a good “signature” of a specific oxidation state of Fe ion. As sodium ions are removed from the fully sodiated structure, the Fe ions are oxidized one by one as indicated by their magnetization changing from $\sim 3.8\mu_0$ to $\sim 4.3\mu_0$, as can be seen in Fig. 3(f) and (g). The same trend appears in the number of d -electrons on each Fe site, which go from $\sim 6\mu_0$ to $\sim 5.6\mu_0$ as sites are oxidized by the removal of Na, see Fig. S1 of the Supplementary Material. It is in perfect analogy with the behavior of the nitrogen-free original NFS structure, as can be seen in Fig. S2 of the Supplementary Material. The voltage profiles from 60 to 180 mA h g^{-1} are driven by Fe redox processes for structures A and B, and we can compare the various curves using usual chemical arguments. In going from 6 to 4 Na atoms per unit cell, Fig. 3(f) and (g) show that Fe sites with nitrogen as nearest neighbors are oxidized. The corresponding average voltages, labeled “second plateau” in Fig. 4, are significantly lower than the average voltage in NFS. This is not surprising as Fe and N form a more covalent bond than the Fe–O one, which leads to a higher energy antibonding d -like orbital on the Fe site. Upon reducing the system, this antibonding orbital becomes occupied, and its higher energy position leads to a lower effective voltage. Further oxidation of the structure involves Fe sites without N near-neighbors for structure A, whereas the Fe sites in structure B still have N near neighbors. Whereas the simple chemical argu-

ment presented previously still applies to structure B, keeping its average voltage relatively low, it no longer holds for structure A and its “first plateau” in Fig. 4 becomes comparable to the average voltage in the N-free structure.

Further desodiation from 2 to 0 Na in the unit cell leads to a different oxidation mechanism. The magnetization of the Fe ions no longer changes, precluding an interpretation based on the simple removal of d -electrons from Fe. The density of states of the structures having 2 Na per unit cell shows that the occupied electronic states near the Fermi level have nitrogen and oxygen character predominantly, as shown in Fig. 5. Further insight into the nature of the oxidation process can be gained by considering the difference in electronic density between a structure with 2 Na ions per unit cell, and the same structure without sodium (no ionic relaxation is allowed in order to compare densities directly). We present this electronic density difference in Figs. S3 and S4 of the Supplementary Material. It can be seen that upon further oxidation, the electronic charge is removed mainly from nitrogen as well as from oxygen ions located on the same tetrahedra as the nitrogen ones. Therefore, the oxidation corresponds to a collective charge removal from the covalent network of oxygen and nitrogen, and not from an atomic-like ionization.

Structure C presents features that are qualitatively different from A and B, with a lower computed voltage profile in Fig. 3(a) and desodiated structures that are less thermodynamically unstable, as seen in Fig. 3(b). The Fe magnetizations shown in Fig. 3(h) indicate that the Fe ions are not oxidized in going from 6 to 3 Na per unit cells; this is further supported by the density of states presented in Fig. 5(c) which confirms that the states oxidized in going from 6 to 3 Na have a dominant nitrogen character. In fact, as can be seen in Fig. S5 of the Supplementary Material, the nitrogen ions are located at nearby interlayer(1) sites; upon desodiation, the structure relaxes significantly bringing the two nitrogen ions in close proximity to form an N_2 bond. Fig. 3(h) reveals that the Fe

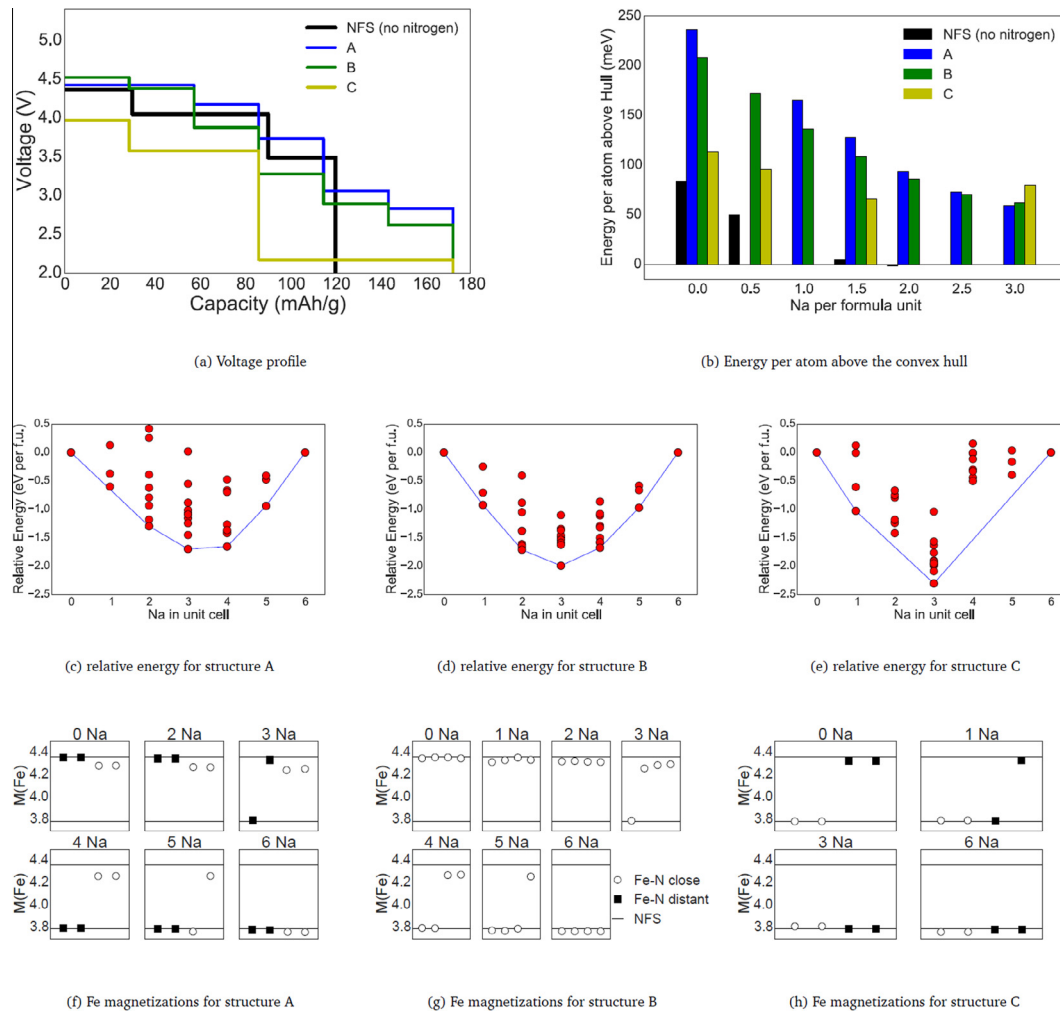


Fig. 3. (a) Computed voltages for structures A, B and C of $\text{Na}_3\text{Fe}_2(\text{SO}_4)_2(\text{SO}_3\text{N})$. The voltage of the substituted structures is compared to that of $\text{Na}_x\text{Fe}_2(\text{SO}_4)_3$. (b) Thermodynamic stability energy for all levels of sodiation. Only structures belonging to the corresponding convex hull are considered, i.e. the absence of a bar signals that no structure with corresponding partial sodiation lies on the hull. (c), (d), (e) Total energy for every partially sodiated structure considered, relative to the energy of a mixture of the corresponding fully sodiated and fully desodiated structures. Lowest energy points are joined by continuous line segments, forming the convex hull: only these points are used to compute the voltage profiles. (f), (g), (h) Computed magnetizations in units of the Bohr magneton for Fe ions in all structures belonging to convex hulls; full squares represent Fe which have a N near neighbor and open circles Fe which do not; horizontal lines show the values obtained in the pristine structure; the Fe sites are listed in order of change in their magnetization.

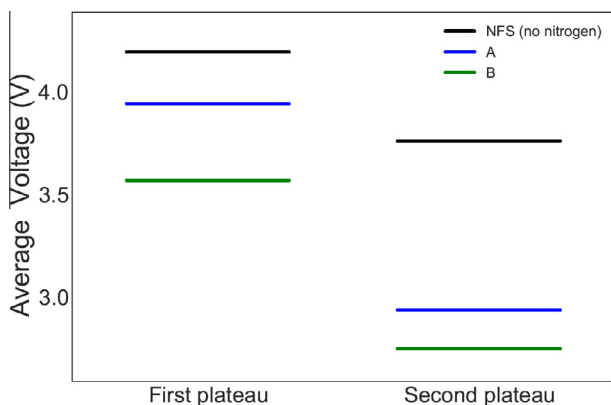


Fig. 4. Average of $\text{Fe}^{2+}/\text{Fe}^{3+}$ voltage plateau from Fig. 3(a) from 0 to 60 mA h g^{-1} and 60–120 mA h g^{-1} for the nitrogen-free structure and from 60 to 115 mA h g^{-1} and 115–170 mA h g^{-1} for structures A and B.

d-orbitals are eventually involved upon further oxidation to 1 and 0 Na per unit cell, leading to voltage plateaux in closer agreement with the other structures.

4. Summary

The use of non-transition-metal redox offers a promising avenue to increase the capacity and energy density of sodium-based intercalation cathode materials. In particular, the introduction of nitrogen in $\text{Na}_x\text{Fe}_2(\text{SO}_4)_3$ to form $\text{Na}_x\text{Fe}_2(\text{SO}_4)_2(\text{SO}_3\text{N})$ could lead to a significant increase in the theoretical energy density from 480 W h kg^{-1} to 650 W h kg^{-1} (structure A). In the most stable structures considered (i.e. A and B), nitrogen mildly affects the redox mechanism based on $\text{Fe}^{2+}/\text{Fe}^{3+}$, and then contributes charge to the further oxidation of the structure once all the iron are in 3+ configurations, in a way similar to what is proposed in $\text{Li}_2\text{FeSiO}_4\text{-N}_y$ [11] although we find no evidence of Fe^{4+} involvement.

This is only a first step, of course, on the pathway to establishing its interest as battery materials. Next steps will require its synthesis to evaluate its ionic conductivity and its cyclability. Irrespective of the final verdict on this specific compound, the general concepts leading to its identification remain.

Indeed, the original structure offers a richness of different chemical environments for oxygen, leading to the possibility of having two nitrogen ions in relative proximity (structure C).

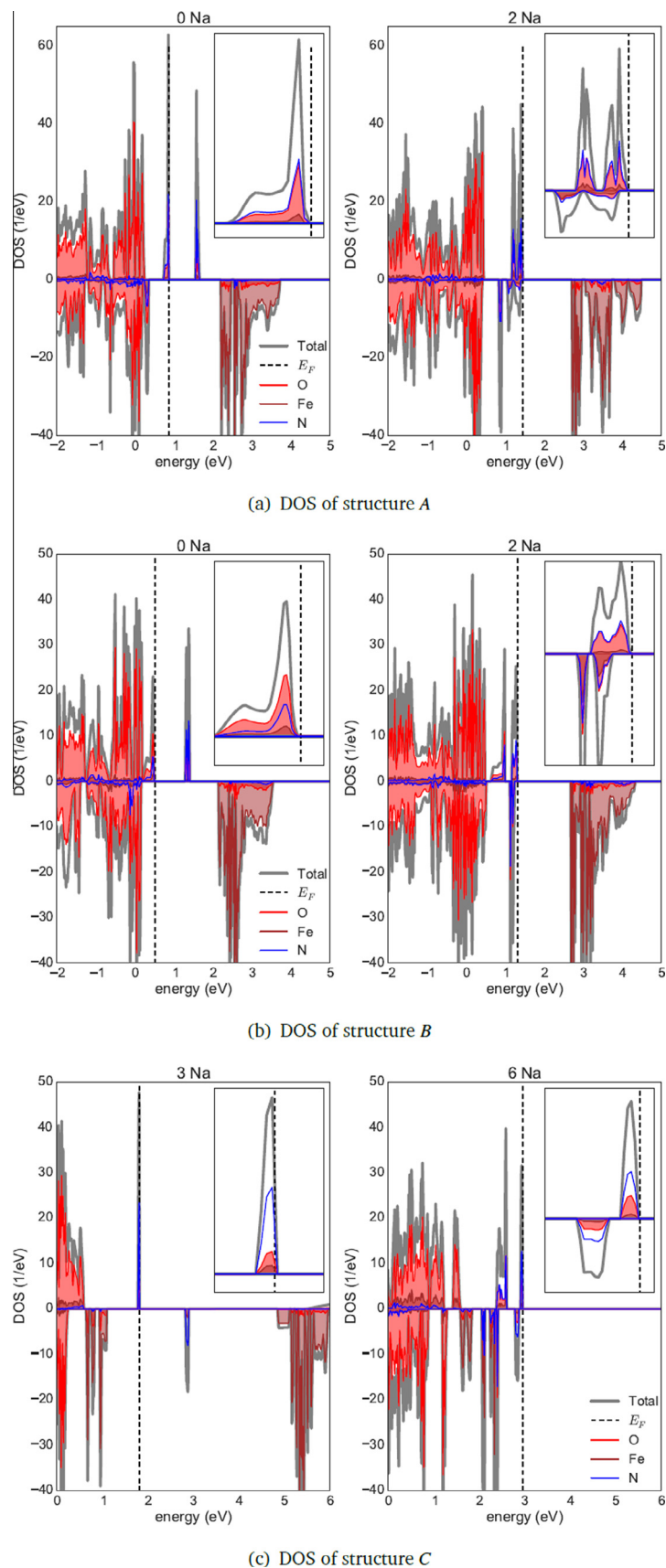


Fig. 5. Densities of states per unit cell near the Fermi level, E_F , for the most stable structures with 0 and 2 Na for structure A and B, and with 3 and 6 Na for structure C. Various colored curves represent projected DOS. The insets show a close up of the density of states near the Fermi energy.

Although not the most stable structure when fully sodiated, the half desodiated structure has comparable excess energy to structure A. While the energy density of structure C, 507 Wh kg^{-1} , is not a significant improvement over the density of the original structure, it does suggest the tantalizing possibility of storing electrical energy in the N_2 bond within a crystalline matrix. If this mechanism could be realized in a transition-metal-free material, the lower voltage implied by this mechanism would certainly be greatly offset by the reduction in weight and cost associated with the freedom from heavy d -electron elements.

Acknowledgments

B.R. thanks Dr. Zimin Feng and Dr. Manuel Smeu for fruitful discussions. V.T. is thankful to Dr. Andrea Paoletta for useful discussions of possible synthesis routes of polyanionic compounds. This work is supported in part by IREQ, MITACS and *Fonds de recherche du Québec – Nature et technologies (FRQ-NT)*. We are grateful to IREQ for providing the computational resources necessary for this project.

Appendix A. Supplementary data

Supplementary data associated with this article can be found, in the online version, at <http://dx.doi.org/10.1016/j.mseb.2016.07.007>.

References

- [1] P. Barpanda, G. Oyama, S.-I. Nishimura, S.-C. Chung, A. Yamada, A 3.8-V earth-abundant sodium battery electrode, *Nat. Commun.* 5 (2014) 4358, <http://dx.doi.org/10.1038/ncomms5358>.
- [2] K. Zaghib, M. Simoneau, Y. Choquette, M. Armand, New lithium insertion electrode materials based on tetraoxoanions derivatives with olivine structure, 1998 Sept 25. CA patent 2200998.
- [3] M. Armand, M. Gauthier, J. Magnan, N. Ravet, Synthesis method for carbon material based on $\text{Li}_x\text{M}_{1-y}\text{M}'_y(\text{XO}_4)_n$, 2003 Feb 12. CA patent 2423129.
- [4] R.V. Noorden, A better battery, *Nature* 507 (2014) 26, <http://dx.doi.org/10.1038/507026a>.
- [5] V. Palomares, P. Serras, I. Villaluenga, K.B. Hueso, J. Carretero-Gonzalez, T. Rojo, Na-ion batteries, recent advances and present challenges to become low cost energy storage systems, *Energy Environ. Sci.* 5 (2012) 5884–5901.
- [6] B.L. Ellis, L.F. Nazar, Sodium and sodium-ion energy storage batteries, *Curr. Opin. Solid State Mater. Sci.* 16 (2012) 168–177, <http://dx.doi.org/10.1016/j.cossms.2012.04.002>.
- [7] N. Yabuuchi, K. Kubota, M. Dahbi, S. Komaba, Research development on sodium-ion batteries, *Chem. Rev.* 114 (2014) 11636–11682, <http://dx.doi.org/10.1021/cr500192f>.
- [8] S.P. Ong, V.L. Chevrier, G. Hautier, A. Jain, C. Moore, S. Kim, X. Ma, G. Ceder, Voltage, stability and diffusion barrier differences between sodium-ion and lithium-ion intercalation materials, *Energy Environ. Sci.* 4 (2011) 3680, <http://dx.doi.org/10.1039/c1ee01782a>.
- [9] M. Sathiyaa, G. Rousse, K. Ramesha, C.P. Laisa, H. Vezin, M.T. Sougrati, M.-L. Doublet, D. Foix, D. Gonbeau, W. Walker, A.S. Prakash, M. Ben Hassine, L. Dupont, J.-M. Tarascon, Reversible anionic redox chemistry in high-capacity layered-oxide electrodes, *Nat. Mater.* 12 (2013) 827–835, <http://dx.doi.org/10.1038/nmat3699>.
- [10] M. Armand, J.-M. Tarascon, M. Arroyo-de Dompablo, Comparative computational investigation of N and F substituted polyoxoanionic compounds, *Electrochem. Commun.* 13 (2011) 1047–1050, <http://dx.doi.org/10.1016/j.elecom.2011.06.027>.
- [11] M. Armand, M.E. Arroyo y de Dompablo, Benefits of N for O substitution in polyoxoanionic electrode materials: a first principles investigation of the electrochemical properties of $\text{Li}_2\text{FeSiO}_{4-y}\text{N}_y$ ($y = 0, 0.5, 1$), *J. Mater. Chem.* 21 (2011) 10026, <http://dx.doi.org/10.1039/c0jm04216a>.
- [12] G. Kresse, J. Furthmüller, Efficiency of ab-initio total energy calculations for metals and semiconductors using a planewave basis set, *Comput. Mater. Sci.* 6 (1996) 15–50, [http://dx.doi.org/10.1016/0927-0256\(96\)00008-0](http://dx.doi.org/10.1016/0927-0256(96)00008-0).
- [13] J.P. Perdew, K. Burke, M. Ernzerhof, Generalized gradient approximation made simple, *Phys. Rev. Lett.* 77 (1996) 3865–3868, <http://dx.doi.org/10.1103/PhysRevLett.77.3865>.
- [14] V.I. Anisimov, F. Aryasetiawan, A.I. Lichtenstein, First-principles calculations of the electronic structure and spectra of strongly correlated systems: the LDA+U method, *J. Phys. Condens. Matter* 9 (1997) 767.
- [15] F. Zhou, M. Cococcioni, C.A. Marianetti, D. Morgan, G. Ceder, First-principles prediction of redox potentials in transition-metal compounds with LDA+U, *Phys. Rev. B* 70 (2004) 235121, <http://dx.doi.org/10.1103/PhysRevB.70.235121>.
- [16] M. Cococcioni, S. de Gironcoli, Linear response approach to the calculation of the effective interaction parameters in the LDA+U method, *Phys. Rev. B* 71 (2005) 035105, <http://dx.doi.org/10.1103/PhysRevB.71.035105>.
- [17] L. Wang, T. Maxisch, G. Ceder, Oxidation energies of transition metal oxides within the GGA+U framework, *Phys. Rev. B* 73 (19) (2006) 195107, <http://dx.doi.org/10.1103/PhysRevB.73.195107>.
- [18] A. Jain, S.P. Ong, G. Hautier, W. Chen, W.D. Richards, S. Dacek, S. Cholia, D. Gunter, D. Skinner, G. Ceder, K.A. Persson, Commentary: the materials project: a materials genome approach to accelerating materials innovation, *APL Mater.* 1 (2013) 011002, <http://dx.doi.org/10.1063/1.4812323>.
- [19] P.E. Blöchl, Projector augmented-wave method, *Phys. Rev. B* 50 (24) (1994) 17953–17979, <http://dx.doi.org/10.1103/PhysRevB.50.17953>.
- [20] G. Kresse, D. Joubert, From ultrasoft pseudopotentials to the projector augmented-wave method, *Phys. Rev. B* 59 (1999) 1758–1775, <http://dx.doi.org/10.1103/PhysRevB.59.1758>.
- [21] M. Aydinol, A. Kohan, G. Ceder, K. Cho, J. Joannopoulos, Ab initio study of lithium intercalation in metal oxides and metal dichalcogenides, *Phys. Rev. B* 56 (3) (1997) 1354–1365, <http://dx.doi.org/10.1103/PhysRevB.56.1354>.
- [22] S.P. Ong, W.D. Richards, A. Jain, G. Hautier, M. Kocher, S. Cholia, D. Gunter, V.L. Chevrier, K.A. Persson, G. Ceder, Python materials genomics (pymatgen): a robust, open-source python library for materials analysis, *Comput. Mater. Sci.* 68 (2013) 314–319, <http://dx.doi.org/10.1016/j.commatsci.2012.10.028>.
- [23] A. Jain, S.P. Ong, W. Chen, B. Medasani, X. Qu, M. Kocher, M. Brafman, G. Petretto, G.-M. Rignanese, G. Hautier, D. Gunter, K.A. Persson, FireWorks: a dynamic workflow system designed for high-throughput applications, *Concurrency Comput. Pract. Experience* 27 (2015) 5037–5059, <http://dx.doi.org/10.1002/cpe.3505>.
- [24] J.A. Kurzman, G. Jouan, M. Courty, M.R. Palacín, M. Armand, N. Recham, Brønsted acid-base reactions with anhydrous sulfamates as a pathway to $[\text{SO}_3\text{N}]^{\ominus}$ -containing compounds: preparation of $\text{Li}_3\text{SO}_3\text{N}$, *Solid State Sci.* 25 (2013) 28–32, <http://dx.doi.org/10.1016/j.solidstatesciences.2013.08.004>.